ARTICLES

Structural mechanism of plant aquaporin gating

Susanna Törnroth-Horsefield[1], Yi Wang[2], Kristina Hedfalk[1], Urban Johanson[3], Maria Karlsson[3], Emad Tajkhorshid[2], Richard Neutze[1] & Per Kjellbom[3]

Plants counteract fluctuations in water supply by regulating all aquaporins in the cell plasma membrane. Channel closure results either from the dephosphorylation of two conserved serine residues under conditions of drought stress, or from the protonation of a conserved histidine residue following a drop in cytoplasmic pH due to anoxia during flooding. Here we report the X-ray structure of the spinach plasma membrane aquaporin SoPIP2;1 in its closed conformation at 2.1 Å resolution and in its open conformation at 3.9 Å resolution, and molecular dynamics simulations of the initial events governing gating. In the closed conformation loop D caps the channel from the cytoplasm and thereby occludes the pore. In the open conformation loop D is displaced up to 16 Å and this movement opens a hydrophobic gate blocking the channel entrance from the cytoplasm. These results reveal a molecular gating mechanism which appears conserved throughout all plant plasma membrane aquaporins.

Water is the medium of life. Because biological membranes have only limited intrinsic water permeability, cells facilitate the flux of water into and out of the cell by means of a family of water-specific membrane protein channels called aquaporins[1]. Members of the aquaporin family are found in archaea, eubacteria and eukaryotes, including fungi, animals and plants. They serve an astonishing variety of physiological functions[2–4] and are easily identified by sequence similarity across all kingdoms of life. In higher eukaryotes, aquaporins are frequently regulated by phosphorylation, pH and osmolarity[2–5]. Aquaporins in plants and animals are highly conserved and form large protein families with 35 members in higher plants[6] and 13 members in humans[3,4,7]. Phylogenetic analyses divide the plant aquaporins into four subfamilies (Supplementary Fig. S1) and their presence in primitive plants such as the bryophyte *Physcomitrella patens* implies that this specialization is ancient[8]. In the model plant *Arabidopsis thaliana* there are 13 well-conserved plasma membrane aquaporins (plasma membrane intrinsic proteins or PIPs) and these further separate into two distinct phylogenetic groups (PIP1 and PIP2).

In plants a large osmotic gradient between the cell interior and exterior can be maintained as a result of the strength of the cellulose microfibril cell wall. The resulting turgor pressure is crucial for many aspects of plant physiology and helps to give plant cells their structure and rigidity. Land plants have evolved to cope with rapid changes in the availability of water by regulating all aquaporins that lie within the plasma membrane (Fig. 1). Closure of the plant plasma membrane aquaporin SoPIP2;1 of spinach (formerly called PM28A (ref. 9)) is triggered by the dephosphorylation of two serine residues: Ser 115 in the cytosolic loop B (conserved as Ser in 12 of the 13 *Arabidopsis* PIPs, and as Thr in one of them) and Ser 274 in the carboxy-terminal region[9,10] (fully conserved in all eight *Arabidopsis* PIP2s). Both residues are situated in consensus phosphorylation sites (Supplementary Fig. S2). Furthermore, the simultaneous closure of all *Arabidopsis* PIPs upon anoxia was recently reported to depend on the protonation of a strictly conserved histidine residue in loop D (ref. 11), which corresponds to His 193 in SoPIP2;1. Distinct chemical signals acting on residues well separated in sequence induce an identical physiological response within PIPs.

A number of high-resolution structures have been reported for water[12–16] and glycerol[17,18] channels, and the mechanism of water and glycerol permeation has been extensively studied with molecular dynamics simulations[18–21]. Nevertheless, plant aquaporin structures have been reported only at low resolution[22,23], and no gating mechanism has been unambiguously demonstrated. Furthermore, the correct assignment of the conformational state of the putative pH-gated channel aquaporin 0 (AQP0) has been controversial[15,16]. To shed light on the molecular mechanism of aquaporin gating, we crystallized and solved the structure of SoPIP2;1 to 2.1 Å resolution, capturing it in its closed conformation. At this resolution the detailed interactions of all residues implicated in gating[9–11] could

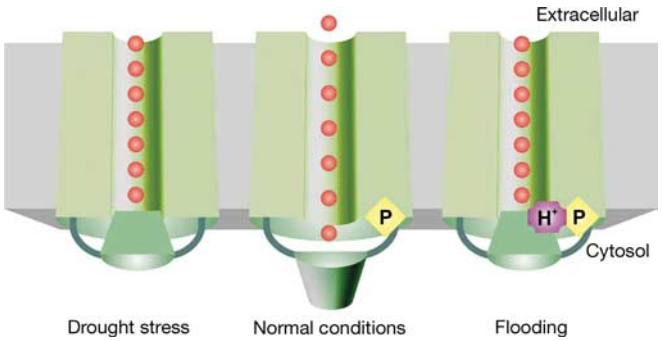

Figure 1 | Diagram illustrating the structural mechanism of aquaporin gating in plant plasma membranes. During drought stress the PIPs close in response to the dephosphorylation of two highly conserved serine residues (Ser 115 and Ser 274 of SoPIP2;1), whereas during flooding they close in response to the protonation of a fully conserved histidine (His 193 of SoPIP2;1).

[1]Department of Chemistry and Bioscience, Chalmers University of Technology, P O Box 462, SE-40530 Göteborg, Sweden. [2]Theoretical and Computational Biophysics Group, Beckman Institute, University of Illinois at Urbana-Champaign, 405 N. Mathews Avenue, Urbana, Illinois 61801, USA. [3]Department of Plant Biochemistry, Lund University, P O Box 124, SE-22100 Lund, Sweden.

be identified. We also determined the X-ray structure of SoPIP2;1 in its open conformation at 3.9 Å resolution, and performed molecular dynamics simulations to examine the initial events leading to the opening of the channel.

Crystal structure of SoPIP2;1

As with all other aquaporin crystals reported so far[12–17], SoPIP2;1 crystallized as a tetramer displaying extended hydrophobic interactions between monomers (Supplementary Fig. S3). In Fig. 2a the open (blue) and closed (green) X-ray structures of SoPIP2;1 are overlaid in stereo on that of bovine AQP0 (ref. 16) (light grey) and AQP1 (ref. 13) (grey). Although animal and plant evolutionary lines separated about 1.6 billion years ago[24], these highly conserved proteins have an identical structural core consistent with the 'hourglass model'[25], differing only by 0.8 Å root-mean-square deviation on C_α atoms within the transmembrane regions. Similarly, the half-helices formed by loops B (cytosolic) and E (extracellular), with the Asn-Pro-Ala (NPA) aquaporin signature motif at the amino-terminal ends, fold into the channel from opposite sides of the membrane and together create a seventh transmembrane region that is perfectly preserved structurally. Seven water molecules are observed within the SoPIP2;1 channel (Supplementary Fig. S4), revealing an unbroken water network stretching almost fully through the pore with a maximum distance of only 3.1 Å between each water molecule. During molecular dynamics simulations these water molecules maintained a stable, continuous, single-file configuration and exhibited a highly correlated motion along the pore axis. As with all other simulated aquaporins[18,19,26], a specific reorientation of water molecules across the NPA motif is observed, strongly indicating the presence of a positive electrostatic potential at the NPA region, which is suggested to prevent proton translocation in aquaporins[27–31].

Conformation of loop D

The most striking difference in the structure of SoPIP2;1 relative to the other aquaporins concerns the conformation of loop D (Fig. 2), which is typically four to seven residues longer for the PIP subfamily members than for other aquaporin homologues (Supplementary Fig. S2). In the closed conformation this extended loop folds underneath the aquaporin and occludes the water pore from accessing the cytosol. A key residue in this respect is the fully conserved Leu 197 of loop D, which inserts into a cavity near the entrance of the channel (Fig. 2a) and, in combination with His 99, Val 104 and Leu 108, creates a hydrophobic barrier blocking the pore. This structural feature is illustrated graphically in Fig. 3b because two water molecules separated by 6.4 Å are clearly visible on either side of the hydrophobic gate associated with Leu 197. Calculations of the pore diameter with the use of HOLE[32] establish that, in the closed conformation, the pore narrows to a diameter of about 1.4 Å at Leu 197 and further narrows to 0.8 Å near Pro 195 and Val 194

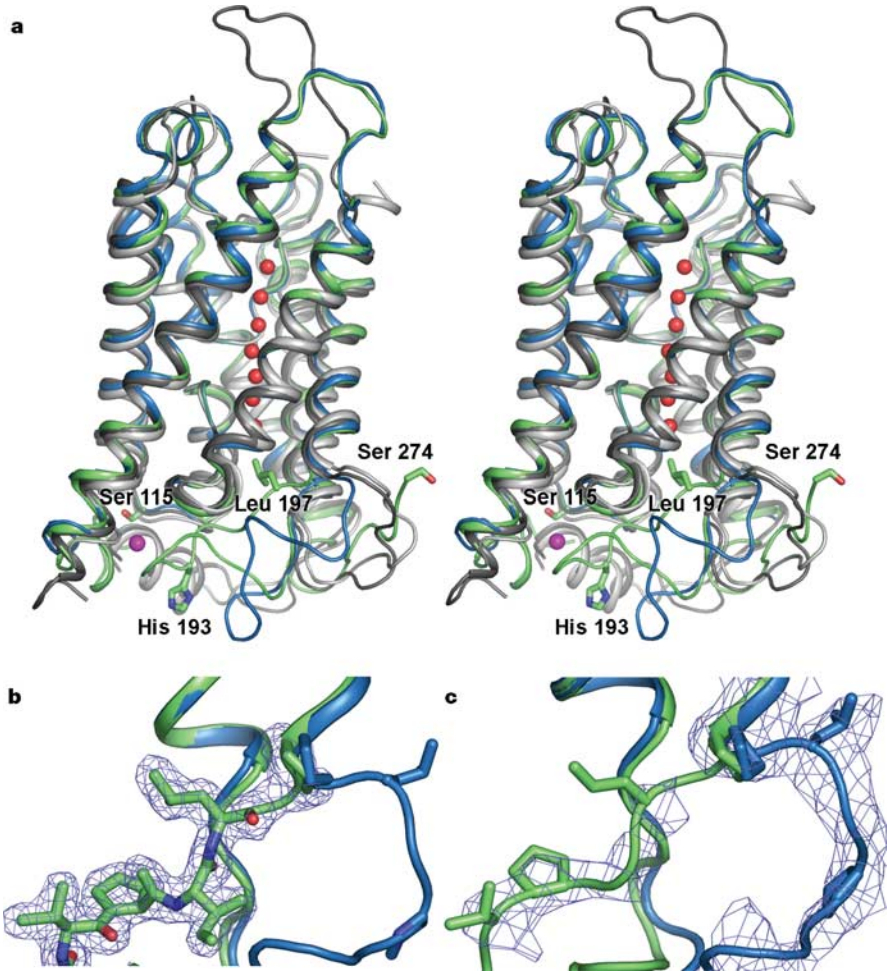

Figure 2 | Structures of the closed and open conformations of SoPIP2;1. **a**, Stereo models of SoPIP2;1 in its open (blue) and closed (green) conformations overlaid on that of AQP0 (light grey; Protein Data Bank (PDB) entry 1YMG) and AQP1 (grey; PDB entry 1J4N). **b**, **c**, Electron density for loop D in the closed (**b**) and open (**c**) conformations. The structural model of the closed conformation is coloured green and the open conformation is coloured blue. Both $2F_o - F_c$ electron density maps are contoured at 1.0σ. Residual electron density in **c** indicates that the closed conformation is also present in partial occupancy.

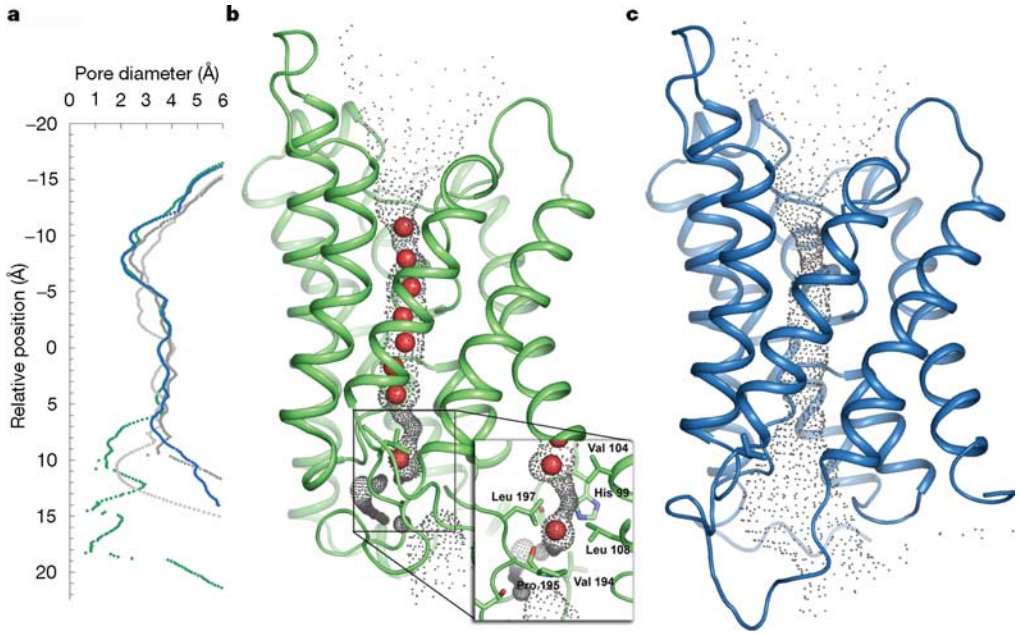

Figure 3 | Characterizing the SoPIP2;1 channel. **a**, The pore diameter of the closed conformation of SoPIP2;1 (green), and the open conformation of SoPIP2;1 (blue), AQP0 (light grey) and AQP1 (grey), represented as a function of the distance from the NPA signature sequence calculated with HOLE[32]. **b**, The same information for the closed conformation of SoPIP2;1 as in **a** but represented as a funnel illustrating the pore boundaries. The inset shows the pore near the gating region of loop D characterized by Leu 197, Pro 195 and Val 194. **c**, The same representation as in **b** but corresponding to the open conformation of SoPIP2;1.

(Fig. 3a, b). This compares with the minimum pore diameter of 2.1 Å within the SoPIP2;1 constriction region and severely restricts the passage of water. Molecular dynamics simulations of the non-phosphorylated protein also record a narrow pore (Fig. 4a) and a very low probability of finding a continuous water file in this region (Fig. 4b).

In the open structure of SoPIP2;1, by contrast, loop D is displaced up to 16 Å and the N terminus of helix 5 extends a further half-turn into the cytoplasm relative to that of its closed-conformation (Fig. 2, and Supplementary Fig. S5), although no hydrogen bond can form between Leu 197 and Pro 201 in the usual $n + 4$ α-helical pattern. The open structure of SoPIP2;1 therefore becomes closer to that of AQP1 (ref. 13) (Figs 2a and 3a). Because of this extension of helix 5, the C_α atoms of Leu 197, Pro 195 and Val 194 are displaced 8.4, 13.9 and 15.0 Å, respectively, away from the cytoplasmic pore entrance (Fig. 2, and Supplementary Fig. S5). Thus, by coupling the movement of loop D to the principal hydrophobic gate that blocks the channel, the pore diameter is locally increased to more than 4 Å (Fig. 3a, c) and the channel is open. A strong conformational coupling between loop D and the hydrophobic gate is clearly

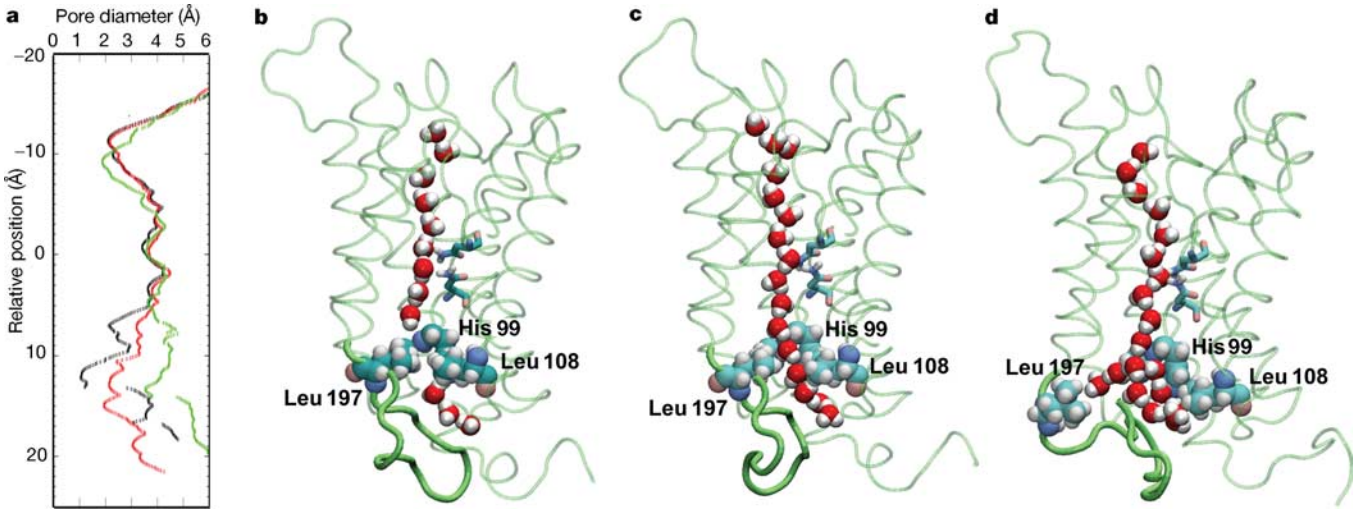

Figure 4 | Results of molecular dynamics simulations of the non-phosphorylated, phosphorylated, and induced open systems. **a**, The pore diameter of the non-phosphorylated (black), phosphorylated (red), and induced open (green) structures calculated with HOLE[32], from structures averaged over the final 5 ns of each simulation. **b**–**d**, Snapshots of simulations of the non-phosphorylated (**b**), phosphorylated (**c**) and induced open (**d**) structures. Loop D is drawn in a thicker tube representation to highlight its conformational coupling to the cytoplasmic gate. Residues forming the cytoplasmic gate are drawn in van der Waals representation. Two asparagine residues of the NPA motifs are shown in stick representation.

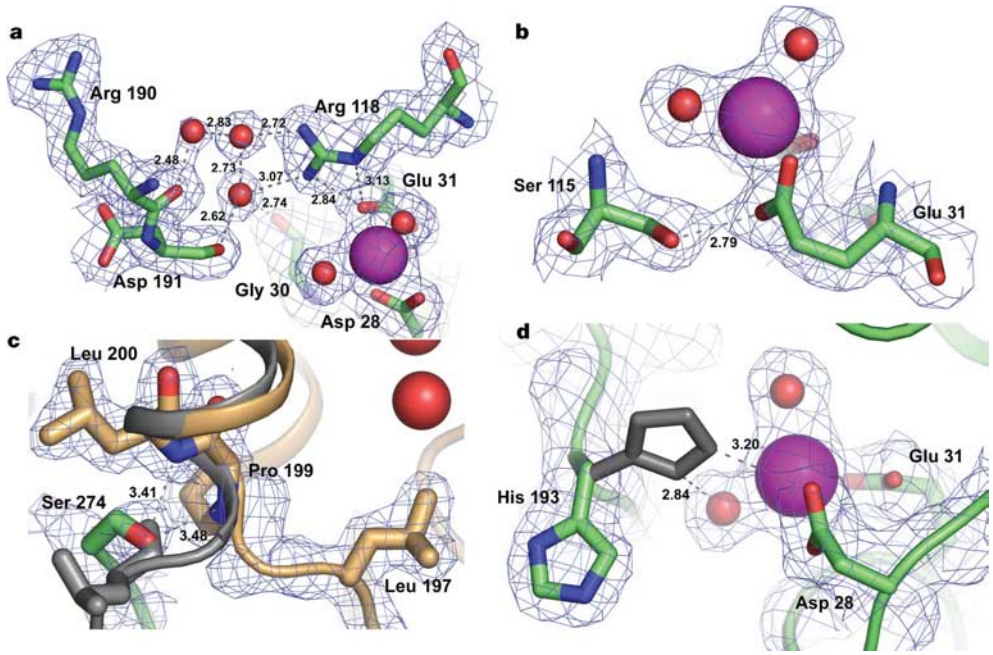

Figure 5 | Electron density at the sites of regulation by phosphorylation and pH for SoPIP2;1 in its closed conformation. **a**, Close-up view of the divalent-cation-binding site showing the location of the Cd^{2+} ion (purple) and the network of hydrogen bonds linking Gly 30 and Glu 31 through Arg 118 to Arg 190 and Asp 191 of loop D. **b**, Close-up view of the phosphorylation residue Ser 115, illustrating its hydrogen bond to Glu 31. **c**, Electron density for Ser 274, which contacts Pro 199 and Leu 200 of a neighbouring monomer of the SoPIP2;1 tetramer. Overlaid in grey is the structure of the open conformation of SoPIP2;1, indicating that a steric clash with Leu 197 prevents helix 5 from adopting this conformation when Ser 274 is dephosphorylated. **d**, Close-up view of His 193. When protonated, an alternative conformation for His 193 (grey) may be adopted that forms a salt bridge to Asp 28. All $2F_o - F_c$ maps are contoured at 1.0σ. Numbers are distances in Å.

observed during molecular dynamics simulations (Fig. 4), in which a partial opening of the gate mediated through the displacement of loop D after phosphorylation of Ser 115 and Ser 274 was observed within 15 ns (Fig. 4a, c). It is also noteworthy that Tyr 149 of AQP0 (ref. 16), which has been suggested to gate AQP0 (refs 15, 33), overlays almost exactly with Leu 197 of SoPIP2;1 (Supplementary Fig. S6). For AQP0, however, only one amino-acid residue blocks the pore, whereas several residues of loop D cap the channel in SoPIP2;1.

Specific interactions governing gating

It has been postulated that divalent cations have a function in aquaporin regulation[9,10] and inhibition[33–35]. In Figs 2a and 5 a heavy metal (coloured purple; Supplementary Fig. S7 shows the anomalous difference density map) is observed near loop D and is assigned as Cd^{2+} because the addition of this ion improved the crystal quality (see Supplementary Information). Cd^{2+} may be replaced by another divalent cation *in vivo*, and a search for similar structural motifs[36] revealed 13 PDB entries containing Ca^{2+} (Supplementary Information gives the accession codes). We therefore propose that this site binds Ca^{2+} *in vivo*. This divalent cation is implicated in regulation because it serves to anchor loop D, through a network involving ionic interactions and hydrogen bonds (Fig. 5a), onto a short α-helix of the N terminus and is critical for defining the closed conformation of SoPIP2;1. Specifically, Arg 190 and Asp 191 of loop D are connected to the side chain of Arg 118 (strictly conserved in PIPs) and Gly 30 through a hydrogen-bond network containing three water molecules. Arg 118 in turn forms hydrogen bonds to Glu 31 (strictly conserved in PIPs), which ligates the Cd^{2+} ion (Fig. 5a, b). Because loop D undergoes a large-scale rearrangement during the transition from the closed to the open conformation

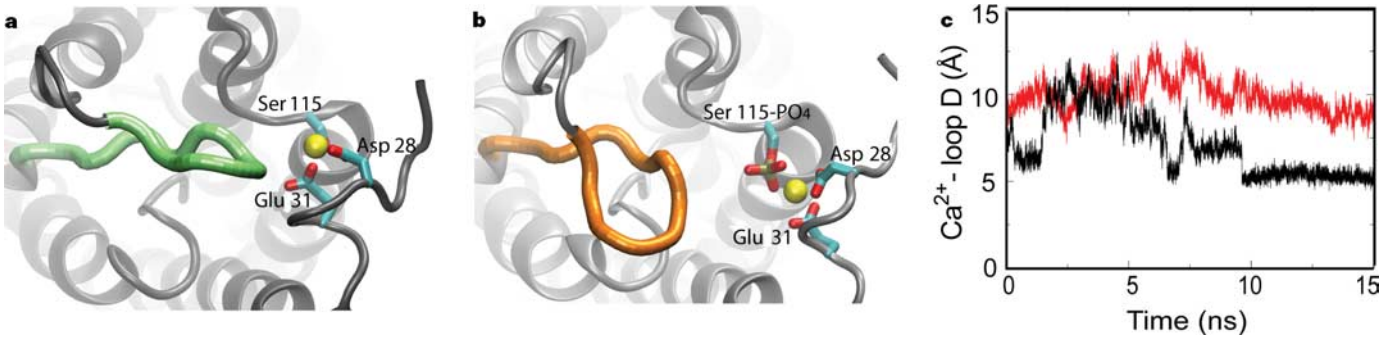

Figure 6 | Regulation of the cytoplasmic entrance into the SoPIP2;1 channel. **a**, **b**, Snapshots from non-phosphorylated (**a**) and phosphorylated (**b**) simulations. The Ca^{2+} ion is shown in yellow van der Waals representation and its coordinating residues (Ser 115, Asp 28 and Glu 31) are shown in stick representation. A mobile fraction of loop D (Ser 188 to Ala 198) is shown in green (**a**) and orange (**b**) tube representation. **c**, The separation of the N terminus and loop D, defined as the distance between the Ca^{2+} ion and the closest C_α atom of loop D. Red, phosphorylated; black, non-phosphorylated.

of SoPIP2;1 (Fig. 2) it is apparent that the phosphorylation of Ser 115 disrupts this network of hydrogen bonds anchoring loop D to the N terminus. The issue of how this disruption evolves is analysed below with molecular dynamics simulations.

The regulatory mechanism of Ser 274 (conserved in PIP2 homologues) can also be understood from our structural results. In this case Ser 274 interacts with the backbone nitrogens of Pro 199 and Leu 200 of an adjacent monomer (Fig. 5c) because the C terminus of SoPIP2;1 extends towards the four-fold axis of the tetramer (Supplementary Fig. S3). From the X-ray structure of the open conformation we observe that, when these interactions are lost, the C terminus is disordered, and the position previously occupied by the side chain of Ser 274 becomes taken by the backbone carbonyl oxygen of Leu 197 (Fig. 5c, grey). Thus a steric clash is removed and the N terminus of helix 5 is able to extend an additional half-turn into the cytoplasm (Fig. 2), thereby displacing Leu 197 and opening the water channel (Fig. 3).

When the aquaporin is open, the protonation of His 193 (strictly conserved in PIPs) closes the channel[11]. A mechanism for pH-regulated PIP gating is also apparent from the closed structure of SoPIP2;1. In Fig. 5d the conformation of His 193 is shown. At low pH, when His 193 is protonated, a simple rotation of the histidine side chain (Fig. 5d, grey) would enable it to form a salt bridge to Asp 28 (conserved in PIPs as Asp or Glu; Supplementary Fig. S2). In this manner the hydrogen-bond-mediated anchor for loop D onto the N terminus (Fig. 5a), which is lost when Ser 115 is phosphorylated, could be recovered. The structure of Ser 115-phosphorylated SoPIP2;1 at low pH can therefore be expected to be rather similar to that of the closed conformation reported here, with the cytoplasmic side of the aquaporin being capped by loop D, and Leu 197, Pro 195 and Val 194 effectively blocking the water channel.

Initial response to serine phosphorylation

To investigate the primary events that trigger the opening of the phosphorylated channel, molecular dynamics simulations of 15 ns duration were performed on the non-phosphorylated protein, and on the protein with both Ser 115 and Ser 274 phosphorylated, both starting from the closed crystal structure. We also conducted a 10-ns simulation starting from the phosphorylated closed structure during which loop D was forced (through constraints applied to residues 182 and 195–198 at the base of the loop; see Supplementary Information) to move towards its conformation in the open crystal structure. For all simulations Cd^{2+} was replaced with Ca^{2+}.

After 10 ns equilibration, the non-phosphorylated protein yielded a stable connection between loop D and the N terminus, as indicated by the short distance (about 5 Å; Fig. 6c) between this loop and the Ca^{2+} ion coordinated by residues in the N terminus (Fig. 6a). Furthermore, the side chains of residues 192–194 on loop D were observed to reorientate towards the N terminus and establish direct and/or water-mediated hydrogen bond interactions with it, primarily through Glu 31. As is typically observed for loops interconnecting transmembrane helices, loop D is a flexible part of the protein and showed considerable fluctuations during the simulations, especially with regard to the position of its amino-acid side chains. Thus, all interactions between loop D and the N terminus observed during these simulations help to anchor this loop onto the cytoplasmic entrance into the pore (Supplementary Fig. S8, green conformation) and thereby decrease the probability of recovering an open channel.

During the 15-ns simulation of the phosphorylated enzyme, a significant rearrangement in the conformation of amino acids coordinating the Ca^{2+} ion occurred. This ion, which was (mainly) coordinated by Asp 28 and one side-chain oxygen of Glu 31 in the non-phosphorylated protein (Fig. 6a), became coordinated by both side-chain oxygens of Asp 28 and Glu 31 as well as the phosphate group of phosphorylated Ser 115 (Fig. 6b). This rearrangement resulted in an average displacement of the ion by 4.7 Å towards the periphery of the aquaporin tetramer in all monomers (Fig. 6b, c) and drew Glu 31 away from its original location, significantly disrupting the hydrogen-bond network connecting loop D to the N terminus. Thus released from its hydrogen-bond-mediated anchor, loop D underwent a significant conformational change away from the cytoplasmic entrance of the pore (Supplementary Fig. S8, orange conformation). Although the amplitude of the movement of loop D observed during this 15-ns simulation was considerably smaller than that observed for the X-ray structure of the open conformation, the nature of this movement (Supplementary Fig. S8, orange conformation) provides a plausible initial trajectory towards the open crystal conformation (Supplementary Fig. S8, blue conformation). We therefore suggest that the conformational change from the closed to the open structure proceeds first through the release of loop D from the N terminus, followed by the extension of the cytoplasmic end of helix 5 on a slower timescale (Fig. 2, and Supplementary Fig. S8).

A specific coupling between the movement of loop D and the opening of the hydrophobic gate near Leu 197 is also evident from simulations (Fig. 4). Before phosphorylation, this gate ($10\,\text{Å} < z < 15\,\text{Å}$; Fig. 4) completely blocks the access of the pore water to the cytoplasm (Fig. 4b) with the minimum diameter of the pore (averaged over the last 5 ns) being 1.04 Å as determined with HOLE[32] (Fig. 4a, black line). After phosphorylation the pore diameter (averaged over the last 5 ns) was significantly increased in this region to 1.94 Å (Fig. 4a, red line) and a stable chain of water molecules connecting the inner channel to the cytoplasm was formed (Fig. 4c). When the loop of the phosphorylated protein was driven towards the loop conformation in the X-ray open structure, the cytoplasmic hydrophobic gate became completely open (average diameter of 3.54 Å over the last 5 ns; Fig. 4a, green line) and the cytoplasmic entrance to the channel became flooded with water (Fig. 4d).

Table 1 | Crystallographic data and refinement statistics

	Closed conformation	Open conformation
Refinement		
Resolution (Å)	40.0–2.1	50.0–3.9
R_{work}/R_{free}	0.181/0.208	0.291/0.332
No. of atoms		
Protein	3756	6874
Ligand/ion	2	
Water	200	
B-factors		
Protein	29.7	69.0
Ligand/ion	30.6	
Water	39.6	
Root-mean-square deviations		
Bond lengths (Å)	0.02	0.024
Bond angles (°)	1.540	2.00

Generality

A deeper understanding of the structural mechanism of water flow regulation provides insight into the unique physiology of plant cells. Structural results and simulations presented here reveal how the extended loop D of SoPIP2;1 containing Leu 197 provides a flexible lid, capping the channel from the cytoplasm and opening a hydrophobic gate after the phosphorylation of Ser 115 and Ser 274. This gating mechanism successfully unifies a significant body of biochemical[9–11] and genetic evidence that has identified specific amino-acid residues governing plant aquaporin gating, and immediately suggests how the closed structure might be stabilized or destabilized. From the high degree of amino-acid sequence conservation this regulatory mechanism seems to be conserved in all plasma membrane aquaporins irrespective of plant species. Thus, the structural mechanism of plant aquaporin gating is applicable to

phenomena as everyday as a neglected pot-plant wilting and the flood irrigation of the rice paddies of Asia.

METHODS

Heterologous membrane protein overexpression. Functional SoPIP2;1, both as His-tagged and non-tagged protein, was overproduced in the methylotrophic yeast *Pichia pastoris*[37]. Purification and concentration protocols are detailed in Supplementary Information.

Crystallization. Crystals of the closed conformation were obtained by hanging-drop vapour diffusion from the non-tagged protein. Sample (1 μl) was mixed 1:1 with the reservoir solution containing 0.1 M Tris-HCl pH 8.0, 30% polyethylene glycol (PEG) 400 and 0.1 M NaCl. 0.1 M $CdCl_2$ was added to the drop in a 1:10 ratio. Crystallization setups were left to equilibrate at 4 °C and crystals appeared within a few days. Crystals of the open conformation were obtained by hanging-drop vapour diffusion from the His-tagged protein. Activity assays on the overexpressed His-tagged protein show significant water transport activity[37]. Sample (1 μl) was mixed 1:1 with the reservoir solution containing 0.1 M sodium citrate pH 5.6, 30% PEG 400 and 0.1 M NaCl. Crystallization setups were left to equilibrate at 4 °C and crystals appeared after six months.

Structure determination of the closed conformation. X-ray diffraction data (Table 1) from the closed conformation to 2.1 Å resolution were recorded at the Swiss Light Source (SLS) beamline X06SA, Villigen, Switzerland. Crystals belong to the space group *I*4, with two molecules in the asymmetric unit. Data were processed using MOSFLM and scaled using SCALA of the CCP4 suite[38]. Molecular replacement was performed with the program MOLREP from the CCP4 program suite[38] with the coordinates of bovine AQP1 (PDB entry 1J4N; ref. 13) as the model. A clear solution with a correlation coefficient and an *R*-factor of 34.3% and 53.1%, respectively, was found. Automated model building was conducted by using ARP/WARP[39] and the resulting model was docked to the correct sequence using GUISIDE[38]. The model was subjected to multiple rounds of refinement in REFMAC5 (ref. 38), NCSREF[38] and CNS[40]. The final *R*-factor and R_{free} are 18.1% and 20.8%, respectively. A single metal-binding site was unambiguously observed as a dominant peak in the anomalous difference density map (Supplementary Fig. S7) and was assigned as Cd^{2+} (see Supplementary Information). The quality of the structure was checked in PROCHECK[41].

Structure determination of the open conformation. X-ray diffraction data (Table 1) from the open conformation to 3.9 Å resolution were collected at the European Synchrotron Radiation Facility (ESRF) beamline ID14 EH2, Grenoble, France. Crystals belong to the space group $P2_12_12$, with four molecules in the asymmetric unit. Molecular replacement was performed as above with the closed conformation as the starting model. A clear solution with a correlation coefficient and *R*-factor of 63.8% and 41.9%, respectively, was found. After the initial rigid-body refinement, only those residues that clearly showed distinct conformations from the closed structure were varied during structural refinement. The C terminus was disordered and could not be assigned. A new conformation for loop D was built into the composite omit $2F_o - F_c$ electron-density map in iterative steps. For each iteration the model was subjected to multiple rounds of refinement in CNS[40] with manual rebuilding in O[42] between each round, and the composite omit map was recalculated. The *R*-factor and R_{free} are 29.1% and 33.2%, respectively. The quality of the structure was checked in PROCHECK[41].

Molecular dynamics simulations. Molecular dynamics simulations were performed with tetrameric models of SoPIP2;1 embedded in a fully hydrated, 100 × 100-$Å^2$ POPE bilayer. Crystallographic water molecules were retained but all Cd^{2+} ions were replaced with Ca^{2+}. The C termini (Ser 274) were capped with amide groups ($CONH_2$) to avoid artificially introducing a negative charge at this critical region. For all simulations the program NAMD2 (ref. 43) and the CHARMM27 parameter set[44,45] were used. The Particle Mesh Ewald method[46] was employed for the computation of electrostatic forces. Langevin dynamics and a Langevin piston were used to maintain the temperature (300 K) and pressure (1 atm), respectively. Model building and analysis were done with VMD[47]. Three systems were simulated: first, the unphosphorylated system, representing a 'closed' channel; second, the 'phosphorylated' channel, in which both Ser 115 and Ser 274 were phosphorylated to trigger the opening; and third, the 'induced open' channel in which C_α coordinates of residues 182 and 195–198 in the open crystal structure were used to induce a fully open structure. After energy minimization and a 500-ps protein-fixed simulation, systems 1 and 2 each were simulated for 15 ns. In system 3, the system was subjected to an additional constrained simulation phase, in which position constraints were applied to C_α atoms of residues 182 and 195–198 in seven 100-ps steps with varying force constants to induce an open structure. After the initial 700 ps of constrained simulation, all constraints were removed and the system was simulated for 10 ns. More details are provided in Supplementary Information.

Received 16 February; accepted 14 October 2005.
Published online 7 December 2005.

1. Preston, G. M., Carroll, T. P., Guggino, W. B. & Agre, P. Appearance of water channels in *Xenopus* oocytes expressing red cell CHIP28 protein. *Science* **256,** 385–387 (1992).
2. Johansson, I., Karlsson, M., Johanson, U., Larsson, C. & Kjellbom, P. The role of aquaporins in cellular and whole plant water balance. *Biochim. Biophys. Acta* **1465,** 324–342 (2000).
3. Agre, P. & Kozono, D. Aquaporin water channels: molecular mechanisms for human diseases. *FEBS Lett.* **555,** 72–78 (2003).
4. King, L. S., Kozono, D. & Agre, P. From structure to disease: the evolving tale of aquaporin biology. *Nature Rev. Mol. Cell Biol.* **5,** 687–698 (2004).
5. Tamas, M. J. *et al.* A short regulatory domain restricts glycerol transport through yeast Fps1p. *J. Biol. Chem.* **278,** 6337–6345 (2003).
6. Johanson, U. *et al.* The complete set of genes encoding major intrinsic proteins in *Arabidopsis* provides a framework for a new nomenclature for major intrinsic proteins in plants. *Plant Physiol.* **126,** 1358–1369 (2001).
7. Morishita, Y., Sakube, Y., Sasaki, S. & Ishibashi, K. Molecular mechanisms and drug development in aquaporin water channel diseases: aquaporin superfamily (superaquaporins): expansion of aquaporins restricted to multicellular organisms. *J. Pharmacol. Sci.* **96,** 276–279 (2004).
8. Borstlap, A. C. Early diversification of plant aquaporins. *Trends Plant Sci.* **7,** 529–530 (2002).
9. Johansson, I. *et al.* Water transport activity of the plasma membrane aquaporin PM28A is regulated by phosphorylation. *Plant Cell* **10,** 451–459 (1998).
10. Johansson, I., Larsson, C., Ek, B. & Kjellbom, P. The major integral proteins of spinach leaf plasma membranes are putative aquaporins and are phosphorylated in response to Ca^{2+} and apoplastic water potential. *Plant Cell* **8,** 1181–1191 (1996).
11. Tournaire-Roux, C. *et al.* Cytosolic pH regulates root water transport during anoxic stress through gating of aquaporins. *Nature* **425,** 393–397 (2003).
12. Murata, K. *et al.* Structural determinants of water permeation through aquaporin-1. *Nature* **407,** 599–605 (2000).
13. Sui, H., Han, B. G., Lee, J. K., Walian, P. & Jap, B. K. Structural basis of water-specific transport through the AQP1 water channel. *Nature* **414,** 872–878 (2001).
14. Savage, D. F., Egea, P. F., Robles-Colmenares, Y., O'Connell, J. D. & Stroud, R. M. Architecture and selectivity in aquaporins: 2.5 Å X-ray structure of aquaporin Z. *PLoS Biol.* **1,** E72 (2003).
15. Gonen, T., Sliz, P., Kistler, J., Cheng, Y. & Walz, T. Aquaporin-0 membrane junctions reveal the structure of a closed water pore. *Nature* **429,** 193–197 (2004).
16. Harries, W. E., Akhavan, D., Miercke, L. J., Khademi, S. & Stroud, R. M. The channel architecture of aquaporin 0 at a 2.2 Å resolution. *Proc. Natl Acad. Sci. USA* **101,** 14045–14050 (2004).
17. Fu, D. *et al.* Structure of a glycerol-conducting channel and the basis for its selectivity. *Science* **290,** 481–486 (2000).
18. Tajkhorshid, E. *et al.* Control of the selectivity of the aquaporin water channel family by global orientational tuning. *Science* **296,** 525–530 (2002).
19. de Groot, B. L. & Grubmuller, H. Water permeation across biological membranes: mechanism and dynamics of aquaporin-1 and GlpF. *Science* **294,** 2353–2357 (2001).
20. Jensen, M. O., Tajkhorshid, E. & Schulten, K. The mechanism of glycerol conduction in aquaglyceroporins. *Structure* **9,** 1083–1093 (2001).
21. Jensen, M. O., Park, S., Tajkhorshid, E. & Schulten, K. Energetics of glycerol conduction through aquaglyceroporin GlpF. *Proc. Natl Acad. Sci. USA* **99,** 6731–6736 (2002).
22. Daniels, M. J., Chrispeels, M. J. & Yeager, M. Projection structure of a plant vacuole membrane aquaporin by electron cryo-crystallography. *J. Mol. Biol.* **294,** 1337–1349 (1999).
23. Kukulski, W. *et al.* The 5 Å structure of heterologously expressed plant aquaporin SoPIP2;1. *J. Mol. Biol.* **350,** 611–616 (2005).
24. Hedges, S. B., Blair, J. E., Venturi, M. L. & Shoe, J. L. A molecular timescale of eukaryote evolution and the rise of complex multicellular life. *BMC Evol. Biol.* **4,** 2 (2004).
25. Jung, J. S., Preston, G. M., Smith, B. L., Guggino, W. B. & Agre, P. Molecular structure of the water channel through aquaporin CHIP. The hourglass model. *J. Biol. Chem.* **269,** 14648–14654 (1994).
26. Wang, Y., Schulten, K. & Tajkhorshid, E. What makes an aquaporin a glycerol channel: A comparative study of AqpZ and GlpF. *Structure* **13,** 1107–1118 (2005).
27. de Groot, B. L., Frigato, T., Helms, V. & Grubmuller, H. The mechanism of proton exclusion in the aquaporin-1 water channel. *J. Mol. Biol.* **333,** 279–293 (2003).
28. Jensen, M. O., Tajkhorshid, E. & Schulten, K. Electrostatic tuning of permeation and selectivity in aquaporin water channels. *Biophys. J.* **85,** 2884–2899 (2003).
29. Chakrabarti, N., Tajkhorshid, E., Roux, B. & Pomes, R. Molecular basis of proton blockage in aquaporins. *Structure* **12,** 65–74 (2004).
30. Ilan, B., Tajkhorshid, E., Schulten, K. & Voth, G. A. The mechanism of proton exclusion in aquaporin channels. *Proteins* **55,** 223–228 (2004).

31. de Groot, B. L. & Grubmüller, H. The dynamics and energetics of water permeation and proton exclusion in aquaporins. *Curr. Opin. Struct. Biol.* **15,** 176–183 (2005).
32. Smart, O. S., Goodfellow, J. M. & Wallace, B. A. The pore dimensions of gramicidin A. *Biophys. J.* **65,** 2455–2460 (1993).
33. Nemeth-Cahalan, K. L. & Hall, J. E. pH and calcium regulate the water permeability of aquaporin 0. *J. Biol. Chem.* **275,** 6777–6782 (2000).
34. Zelenina, M., Bondar, A. A., Zelenin, S. & Aperia, A. Nickel and extracellular acidification inhibit the water permeability of human aquaporin-3 in lung epithelial cells. *J. Biol. Chem.* **278,** 30037–30043 (2003).
35. Zelenina, M., Tritto, S., Bondar, A. A., Zelenin, S. & Aperia, A. Copper inhibits the water and glycerol permeability of aquaporin-3. *J. Biol. Chem.* **279,** 51939–51943 (2004).
36. Madsen, D. & Kleywegt, G. J. Interactive motif and fold recognition in protein structures. *J. Appl. Crystallogr.* **35,** 137–139 (2001).
37. Karlsson, M. *et al.* Reconstitution of water channel function of an aquaporin overexpressed and purified from *Pichia pastoris*. *FEBS Lett.* **537,** 68–72 (2003).
38. Bailey, S. The CCP4 suite: programs for protein crystallography. *Acta Crystallogr. D* **50,** 760–763 (1994).
39. Morris, R. J., Perrakis, A. & Lamzin, V. S. ARP/wARP and automatic interpretation of protein electron density maps. *Methods Enzymol.* **374,** 229–244 (2003).
40. Brunger, A. T. *et al.* Crystallography and NMR system: A new software suite for macromolecular structure determination. *Acta Crystallogr. D* **54,** 905–921 (1998).
41. Laskowski, R. A., Rullmannn, J. A., MacArthur, M. W., Kaptein, R. & Thornton, J. M. AQUA and PROCHECK-NMR: programs for checking the quality of protein structures solved by NMR. *J. Biomol. NMR* **8,** 477–486 (1996).
42. Jones, T. A., Zou, J.-Y., Cowan, S. W. & Kjeldgaard, M. Improved methods for building protein models in electron density maps and the location of errors in these models. *Acta Crystallogr. A* **47,** 110–119 (1991).
43. Kalé, L. *et al.* NAMD2: Greater scalability for parallel molecular dynamics. *J. Comp. Phys.* **151,** 283–312 (1999).
44. MacKerell, A. D. *et al.* All-atom empirical potential for molecular modeling and dynamics studies of proteins. *J. Phys. Chem. B* **102,** 3586–3616 (1998).
45. Schlenkrich, M., Brickmann, J., MacKerell, A. D. & Karplus, M. in *Biological Membranes: A Molecular Perspective from Computation and Experiment* (eds Merz, K. M. & Roux, B.) 31–81 (Birkhauser, Boston, Massachusetts, 1996).
46. Darden, T., York, D. & Pedersen, L. Particle Mesh Ewald—an *N*.log(*N*) method for Ewald sums in large systems. *J. Chem. Phys.* **98,** 10089–10092 (1993).
47. Humphrey, W., Dalke, A. & Schulten, K. VMD: visual molecular dynamics. *J. Mol. Graph.* **14,** 33–38 (1996).

Supplementary Information is linked to the online version of the paper at www.nature.com/nature.

Acknowledgements We thank C. Larsson for useful discussions; the Pittsburgh Supercomputer Center and the National Center for Supercomputing Applications for providing computer time; and the European Synchrotron Radiation Facility and the Swiss Light Source for access to synchrotron radiation. Financial support was provided by Formas, the Research School of Pharmaceutical Sciences (FLÄK), Swegene, the Swedish Research Council (VR), the Swedish Strategic Research Foundation (SSF), the European Commission Integrated Projects EMEP and SPINE, the Chalmers Bioscience Programme and the NIH.

Author Information The coordinates and structure factor amplitudes for the closed and open structures have been deposited in the Protein Data Bank under the accession codes 1Z98 and 2B5F, respectively. Reprints and permissions information is available at npg.nature.com/reprintsandpermissions. The authors declare no competing financial interests. Correspondence and requests for materials should be addressed to R.N. (richard.neutze@chembio.chalmers.se), P.K. (per.kjellbom@plantbio.lu.se) or E.T. (emad@ks.uiuc.edu).